Progress In Electromagnetics Research C, Vol. 126, 105–123, 2022

An Improved Low Switching Frequency Three-Vector Model Predictive Torque Control Strategy for Permanent Magnet Synchronous Motors

Qianghui Xiao[1], Zhe Li[1], Yang Zhang[1, *], Bing Luo[2], and Tingting Wang[2]

Abstract—In order to further reduce the computational complexity as well as the average switching frequency of the inverter for model predictive torque control (MPTC), an improved MPTC control strategy for a three-vector low switching frequency based permanent magnet synchronous motor is proposed. Firstly, an analysis is conducted on the combined effect of the torque and magnetic chain based on the three voltage vectors, based on which the vector combinations are matched to form an offline optimized switching table, and then the three voltage vector combinations are selected from the offline optimized switching table according to the torque control requirements in order to reduce the amount of system calculations. Then, on this basis, a hysteresis loop technique for direct torque control is introduced to reduce the average switching frequency of the inverter. An improved MPTC control strategy with a fuzzy variable hysteresis loop width is further proposed to fuzzy control the dynamic output hysteresis loop width scaling factor according to the motor operating state. Experimental results show that the improved MPTC control strategy with fuzzy variable hysteresis loop width results in optimal combined average switching frequency and current harmonics with reduced computational effort.

1. INTRODUCTION

Model Predictive Torque Control (MPTC) has simple idea, fast dynamic response, and selects the combination of voltage vectors with the smallest cost function from the alternative vectors as the optimal output. In recent years, it has gradually become the control field of Permanent Magnet Synchronous Motor (PMSM) research [1–4].

Based on the number of voltage vectors acting in the control cycle, MPTC can be divided into single-vector [5], double-vector [6], and triple-vector [7–9] control strategies. Single vector control is simple, but torque pulsation is high. Double vectors improve the torque pulsation, but cannot meet the higher requirements of the motor for torque control [7]. Based on the above, this paper investigates the three-vector MPTC.

Ref. [8] proposes a three-vector improved MPTC control strategy for constructing virtual vector sets, but raises the computational effort of the controller. Ref. [9] used the enumeration method to first calculate the first effective vector and then calculate the second effective vector based on the sector where the first effective vector is located. The shortcoming of this strategy is that it increases the computation time of the controller in one cycle. Refs. [10, 11] eliminated some vectors, and selected the remaining vectors to build an optimized offline switch table, which saved calculation time, but still required multiple online rolling calculations, and the calculation burden needed to be further reduced.

Received 5 September 2022, Accepted 14 October 2022, Scheduled 3 November 2022
* Corresponding author: Yang Zhang (459387623@qq.com).
[1] Hunan University of Technology, Zhuzhou 412007, China. [2] CSG Electric Power Research Institute Co. Ltd, Guangzhou, Hunan Province, China.

Some literatures have proposed the method of using virtual voltage vector to increase the finite voltage vector set, which can obtain better torque performance, but its disadvantage is that the computational burden needs to be further reduced [12–14]. Reference [15] proposed a three-vector model predictive torque control strategy that eliminates the weight coefficient, which avoids the problem of finding the optimal value of the weight coefficient in the traditional value function after multiple tests and reduces the computational complexity of the system. Reference [16] added an additional effective vector based on traditional MPTC to reduce the problem of flux linkage fluctuation, but it increases the computational complexity of the system. References [17] designed a new type of switch meter to effectively reduce the torque ripple. Reference [18] proposed a model predictive torque control based on sliding mode control to improve the robustness of the drive system but to reduce the amount of system computation.

Reducing the switching frequency is of great significance for reducing switching losses and improving motor control efficiency. Traditional model predictive torque control generally does not consider the switching frequency problem. Reference [19] aimed to reduce the switching times and reduces some of the alternative voltage vectors with large switching times, but does not consider the impact of this control strategy on system performance. Reference [20] proposed a strategy of fixed hysteresis width based on the direct torque control strategy. Although the switching frequency is reduced, it cannot adapt to complex and changeable operating conditions. Reference [21] proposed an MPTC strategy with hysteresis control, but the multi-step prediction method given in this paper has a large amount of computation, which is difficult to implement on a low-cost DSP platform.

To address the above problems, this paper proposes an improved three-vector low-switching frequency three-vector MPTC strategy using a table-mounted permanent magnet synchronous motor as the research object. The enumeration method is used to calculate the action time of the three vectors in one cycle, and the six alternative vectors in the conventional torque prediction are reduced to four. Finally, the optimal voltage vector is selected by the principle of cost function minima. At the same time, the search method is used to determine the control strategy of the fixed hysteresis width. Furthermore, the MPTC control strategy of fuzzy variable hysteresis loop width is proposed to improve the current harmonic THD (Total Harmonic Distortion) under the premise of reducing the average switching frequency. The effectiveness of the proposed control strategy is verified by MATLAB/Simulink simulation and hardware in the loop simulation experiments.

2. MATHEMATICAL MODEL OF SPMSM

In this paper, surface permanent magnet synchronous motor (SPMSM) assumes symmetrical and star-connected stator three-phase windings, neglecting core losses, and a rotor without damped windings. Based on the above ideal assumptions, the PMSM voltage equation is expressed in the dq coordinate system as [22]:

$$\begin{bmatrix} u_d \\ u_q \end{bmatrix} = \begin{bmatrix} R_s & 0 \\ 0 & R_s \end{bmatrix} \begin{bmatrix} i_d \\ i_q \end{bmatrix} + \omega \begin{bmatrix} -\psi_d \\ \psi_q \end{bmatrix} + p \begin{bmatrix} \psi_d \\ \psi_q \end{bmatrix} \tag{1}$$

The equation for the magnetic chain in this case is

$$\begin{bmatrix} \psi_d \\ \psi_q \end{bmatrix} = \begin{bmatrix} L_s & 0 \\ 0 & L_s \end{bmatrix} \begin{bmatrix} i_d \\ i_q \end{bmatrix} + \begin{bmatrix} \psi_f \\ 0 \end{bmatrix} \tag{2}$$

The electromagnetic torque equation is:

$$T_e = \frac{3}{2} p_n \psi_f i_q \tag{3}$$

In the formulas, u_d, u_q are the crossed straight axis stator voltages; i_d, i_q are the stator currents; ψ_d, ψ_q are for stator magnetic chain; ω is the electrical angular velocity; ψ_f is the magnetic chain of permanent magnets; SPMSM inductance $L_d = L_q = L_s$; R_s is the resistance of the stator winding; p is the differential operator.

3. IMPROVED MODEL PREDICTIVE TORQUE CONTROL

The improved three-vector MPTC strategy is based on the torque control requirements, and the three-voltage vector combination is selected by an offline optimized switching table to reduce the number of

alternative vectors to reduce the computational burden and reduce the harmonics of the current. The strategy can be divided into the selection of the three voltage vector combinations, the calculation of the duration of the voltage vectors in one cycle according to the given calculation, and the design of the cost function.

3.1. Voltage Vector Combination Selection

The MPTC based on three vectors consists of three voltage vectors in one sampling period, two valid vectors, and one zero vector. Instead of calculating u_{out} in advance and then calculating the second valid vector by enumeration, the method used in this paper reduces the amount of calculation by judging the sector in which the predicted given value is located by offline optimum switching tables to select the combination of the three voltage vectors. A first-order Eulerian discretization of Equations (1) and (3) shows that:

$$i_q(k+1) = \left(1 - \frac{R_s T_s}{L_s}\right) i_q(k) - \frac{T_s}{L_s}\omega_e L_d i_d(k) - \frac{T_s}{L_s}\omega_e \psi_f + \frac{T_s}{L_s} u_q(k) \tag{4}$$

$$u_q(k+1) = \frac{L_s}{T_s}\left(\frac{T_{e\_ref}}{1.5 P_n \psi_f} - M\right) \tag{5}$$

To simplify the formula, make $M + u_q(k)T_s/L_s = i_q(k+1)$and $T = u_q(k+1)$. According to Equations (1), (4), and (5):

$$u_\beta = u_\alpha \tan\theta + T/\cos\theta \tag{6}$$

When θ and torque are given to change, that is, when $\tan\theta$ and $T/\cos\theta$ are changed, under the $\alpha\beta$ axis, Equation (6) will have intersection with the four effective vectors in the spatial voltage vector, that is, to satisfy increasing or decreasing torque and magnetic chain. The offline optimized vector combination selection table is formed as shown in Table 1.

Table 1. Off-line optimisation vector combination selection table.

$\tan\theta$	$T/\cos\theta$	Combination selection
$[0, \sqrt{3}]$	> 0	$u_{2,3}/u_{2,4}/u_{3,5}/u_{3,4}$
$[0, \sqrt{3}]$	< 0	$u_{1,2}/u_{2,6}/u_{5,6}/u_{15}$
$\sqrt{3}, +\infty]$	> 0	$u_{1,2}/u_{1,3}/u_{1,6}/u_{2,6}$
$\sqrt{3}, +\infty]$	< 0	$u_{3,4}/u_{3,5}/u_{4,5}/u_{4,6}$
$(-\sqrt{3}, 0]$	> 0	$u_{1,2}/u_{1,3}/u_{2,3}/u_{2,4}$
$(-\sqrt{3}, 0]$	< 0	$u_{1,6}/u_{1,5}/u_{5,6}/u_{4,6}$
$[-\infty, -\sqrt{3}]$	> 0	$u_{1,2}/u_{2,6}/u_{1,6}/u_{1,5}$
$[-\infty, -\sqrt{3}]$	< 0	$u_{2,3}/u_{3,5}/u_{3,4}/u_{2,4}$

Taking $\tan\theta \in [0, \sqrt{3}]$ and $T/\cos\theta > 0$ as examples, the first to-be-selected vector and the second to-be-selected vector will be chosen from 3, 4, and 4, and the third voltage vector will be the zero vector. According to Equation (6), the four combinations are (u_3, u_4), (u_3, u_2), (u_3, u_5), and (u_2, u_5). The optional voltage vector range coverage after the synthesis of the four voltage vector combinations is shown in Fig. 1. Taking (u_3, u_4, u_7) as an example, the direction of the synthesized voltage vector as well as the amplitude can be changed when each voltage vector acts for different times.

3.2. Time Distribution of the Voltage Vector

Using the torque and chain-free differential beat control strategy from the literature [15], the action time of each of the three vectors in a control cycle is calculated. The voltage vector action diagram is shown in Fig. 2.

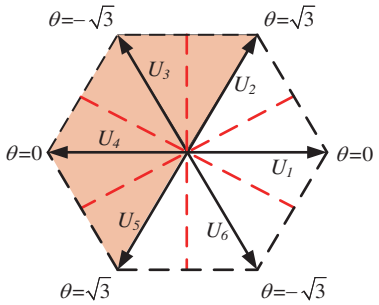

Figure 1. Schematic diagram of improved MPTC selectable voltage vector range.

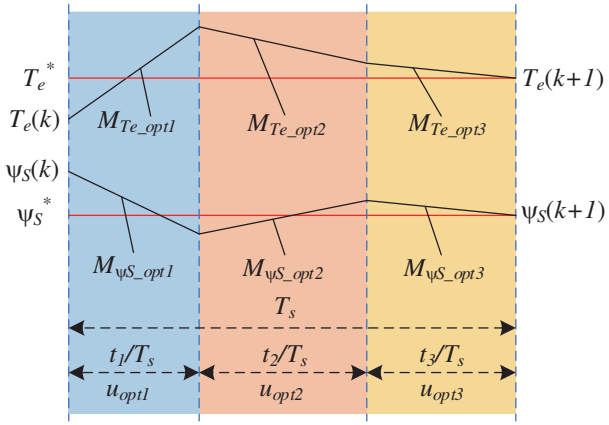

Figure 2. Diagram of voltage vector action.

$$\begin{cases} M_{T_{e\_out1}} = \dfrac{T_e(k+1)_{out1} - T_e(k)}{T_s} \\ M_{\psi_{s\_out1}} = \dfrac{\psi_s(k+1)_{out1} - \psi_s(k)}{T_s} \\ M_{T_{e\_out2}} = \dfrac{T_e(k+1)_{out2} - T_e(k)}{T_s} \\ M_{\psi_{s\_out2}} = \dfrac{\psi_s(k+1)_{out2} - \psi_s(k)}{T_s} \\ M_{T_{e\_out3}} = \dfrac{T_e(k+1)_{out3} - T_e(k)}{T_s} \\ M_{\psi_{s\_out3}} = \dfrac{\psi_s(k+1)_{out3} - \psi_s(k)}{T_s} \end{cases} \tag{7}$$

Equation (7) calculates the rate of change of torque and magnetic chain under the action of the three voltage vectors in the three-vector control, $T_e(k+1)_{out1}$, $T_e(k+1)_{out2}$, $T_e(k+1)_{out3}$, $\psi_s(k+1)_{out1}$, $\psi_s(k+1)_{out2}$ and $\psi_s(k+1)_{out3}$ as the predicted values of torque and magnetic chain under the action of the three voltage vectors u_{out1}, u_{out2} and u_{out3}, respectively. $T_e(k)$ and $\psi_s(k)$ are the torque value and flux linkage value at the current moments.

Difference-free beat control is used in one cycle so that the torque and chain predictions reach the given values $T_{e\_ref}(k)$ and $\psi_{s\_ref}(k)$, satisfying:

$$\begin{cases} T_e(k+1) = T_{e\_ref} = T_e(k) + M_{T_{e\_out1}} t_1 + M_{T_{e\_out2}} t_2 + M_{T_{e\_out3}} t_3 \\ |\psi_s(k+1)| = \psi_{s\_ref} = |\psi_s(k)| + M_{\psi_{s\_out1}} t_1 + M_{\psi_{s\_out2}} t_2 + M_{\psi_{s\_out3}} t_3 \end{cases} \tag{8}$$

In the formula, $t_3 = T_s - t_1 - t_2$; T_{e_ref} and ψ_{s_ref} are the given values of torque and flux linkage.

The combination of the three vectors for the corresponding moment is selected from Equation (6), and then the final $T_e(k+1)$ and $\psi_s(k+1)$ predicted values are calculated according to Equation (7) and Equation (8).

3.3. Duty Cycle Assignment

In this paper, we adopt the torque and magnetic chain without differential beat control strategy, which eliminates the weight coefficient and simplifies the cost function. The value function is therefore designed as follows:

$$g = |T_e(k+1) - T_{e\_ref}| \tag{9}$$

The analysis is based on the comprehensive effect of the three voltage vectors on the torque and flux linkage, and on this basis, the vector combination matching is performed to form an optimized switch table. Then according to the torque control requirements, the off-line optimization switch table is used to select the three-voltage vector combination to reduce the system calculation amount.

3.4. Introduction of Hysteresis

In a permanent magnet synchronous motor inverter system, the switching losses of the power devices occupy a major part of the inverter losses, so the switching frequency of the inverter needs to be controlled at a low level without weakening the control performance. However, conventional MPTC uses the minimum error in the predicted torque as the selection criterion for the optimal vector, which often results in an increase in the switching frequency of the system. The introduction of the hysteresis loop concept in MPC control allows the construction of MPTC control with hysteresis loops. By introducing the concept of hysteresis loop in MPC control, the tracking performance and switching frequency of the controller are adjusted by selecting an appropriate hysteresis loop bandwidth to constrain the stator magnetic chain amplitude and electromagnetic torque inside the hysteresis loop and keep the output vector constant when it does not exceed the hysteresis loop bandwidth, thus allowing the system to operate at a lower average switching frequency condition.

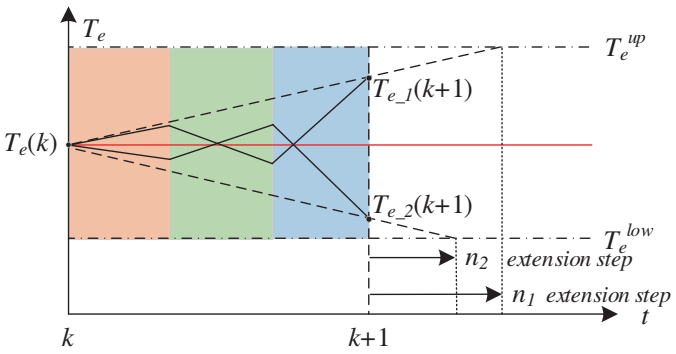

Figure 3. The action diagram of hysteresis MPTC voltage vector.

Figure 3 shows the optimal vector selection strategy for the MPTC after the introduction of the hysteresis loop. The upper and lower bounds, T_e^{up} and T_e^{low}, of the hysteresis loop are first constructed around the given values of T_{e_ref} in the outer loop, and the electromagnetic torque $T_e(k)$ can be observed from the sampled values of the stator current and speed when $t = k$. The predicted value of the electromagnetic torque $T_e(k+1)$ for each candidate vector at moment $t = k+1$ can be obtained from the modified MPTC used in the previous section.

After the introduction of the hysteresis loop, the optimal vector is no longer chosen by the minimum value of the cost function as the evaluation criterion, but by the longest length that can be extended

within the hysteresis loop, when the cost function is constructed in the following form.

$$n = \begin{cases} \dfrac{T_e^{up} - T_e(k+1)}{T_e(k+1) - T_e(k)}, & Te(k+1) > Te(k) \\ \dfrac{T_e^{low} - T_e(k+1)}{T_e(k+1) - T_e(k)}, & Te(k+1) < Te(k) \end{cases} \tag{10}$$

The length that each candidate vector can be extended in the hysteresis loop is determined by the smaller of torque and magnetic chain. After the introduction of the hysteresis loop, the optimal vector is no longer selected based on the minimum tracking error as the evaluation index, but on the longest extension in the hysteresis loop as the selection criterion, and the cost function is then constructed in the following form:

$$g = n \tag{11}$$

As in Fig. 3, $T_e\_2(k+1)$ has the least error from the reference value, but at this point $T_e\_1(k+1)$ can extend longer inside the hysteresis loop, so $T_{e\_1}(k+1)$ will be selected as the optimal vector output.

The composition of the upper and lower bounds in hysteresis loop control reflects the importance of the control target in reducing the switching frequency, and the width of its hysteresis loop will have a direct impact on the performance of the system. Therefore, it is crucial to design a reasonable hysteresis loop width to optimize motor performance.

Define the RMSE (Root Mean Squared Error) of the torque pulsation, the average switching frequency and the average error of the speed as:

$$T_{e\_RMSE} = \sqrt{\frac{\sum_{i=1}^{n} (Te - Te\_ref)^2}{n}} \tag{12}$$

$$f_{ave} = \frac{N_{switch}}{6t} \tag{13}$$

$$\Delta N = \frac{N_{ref} - N_{back}}{t_m} \tag{14}$$

where n is the total number of sampling points at simulation time; N_{switch} is the total number of inverter switches; t is the total sampling time; t_m is the steady-state error after loading.

The design of the hysteresis loop is obtained by repeated trials, given a motor reference speed of 2000 r/min, a load torque of 0.1 Nm, and a simulation time duration of 0.4 s. Using 0 times the current moment's given torque value as the upper and lower boundaries of the hysteresis loop, the width of the hysteresis band is gradually increased in appropriate step multiples (0.01 times in this paper). The results are shown in Table 2 and Figs. 4 to 7.

The MPTC simulation model of SPMSM is built in MATLAB/Simulink. The sampling period of the simulation model is 1×10^{-6} s; the DC bus voltage is 24 V. The SPMSM parameters for simulation are shown in Table 4.

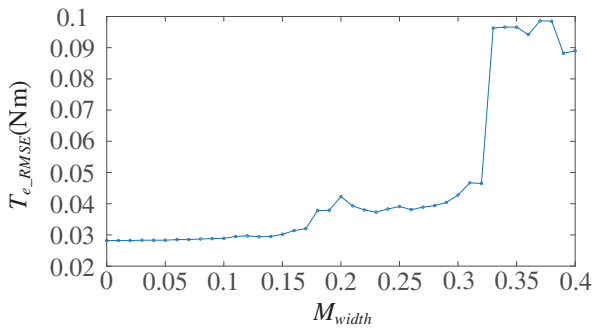

Figure 4. RMS torque ripple under different error bands.

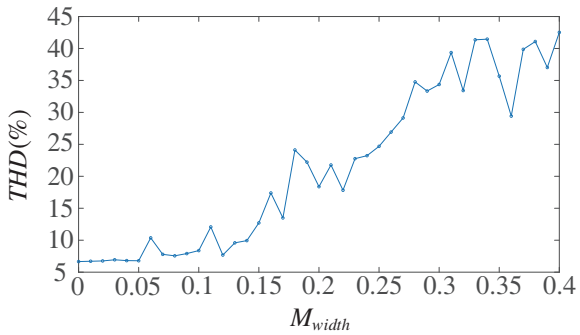

Figure 5. Current harmonic THD under different error bands.

Table 2. Motor system performance for various hysteresis loop widths.

M_{width}	T_{e_RMSE} (Nm)	THD (%)	f_{ave} (kHz)	ΔN (r/min)	M_{width}	T_{e_RMSE} (Nm)	THD (%)	f_{ave} (kHz)	ΔN (r/min)
0	0.0282	6.66	11.221	0.2096	0.21	0.0393	21.77	10.341	0.1386
0.01	0.0282	6.71	11.228	0.2256	0.22	0.0380	17.82	10.196	0.1717
0.02	0.0282	6.76	11.218	0.2218	0.23	0.0373	22.76	9.980	0.3958
0.03	0.0283	6.94	11.202	0.2310	0.24	0.0383	23.23	9.878	0.1413
0.04	0.0283	6.81	11.199	0.2316	0.25	0.0391	24.69	9.747	0.1955
0.05	0.0283	6.79	11.139	0.2249	0.26	0.0381	26.92	9.777	0.3872
0.06	0.0285	10.37	11.129	0.2491	0.27	0.0389	29.13	9.609	0.4963
0.07	0.0285	7.79	11.128	0.2437	0.28	0.0394	34.77	9.484	0.5626
0.08	0.0287	7.56	11.105	0.2653	0.29	0.0404	33.34	9.528	0.3690
0.09	0.0288	7.91	11.107	0.2448	0.30	0.0428	34.37	9.372	0.4322
0.10	0.0289	8.38	11.008	0.2562	0.31	0.0467	39.36	9.148	0.7121
0.11	0.0295	12.08	11.114	0.2403	0.32	0.0465	33.42	9.248	0.5433
0.12	0.0297	7.68	11.021	0.2617	0.33	0.0963	41.36	9.015	0.7140
0.13	0.0294	9.59	11.056	0.2474	0.34	0.0966	41.46	8.959	0.9344
0.14	0.0295	9.94	11.012	0.2185	0.35	0.0966	35.67	8.914	0.9311
0.15	0.0302	12.71	10.899	0.2574	0.36	0.0942	29.42	8.800	1.1757
0.16	0.0314	17.39	10.861	0.2663	0.37	0.0986	39.87	8.699	1.4466
0.17	0.0320	13.49	10.768	0.2481	0.38	0.0985	41.09	8.612	1.3996
0.18	0.0378	24.12	10.571	0.2682	0.39	0.0882	37.03	8.535	1.6113
0.19	0.0379	22.22	10.500	0.1929	0.40	0.0890	42.52	8.421	1.9909
0.20	0.0423	18.38	10.393	0.2484					

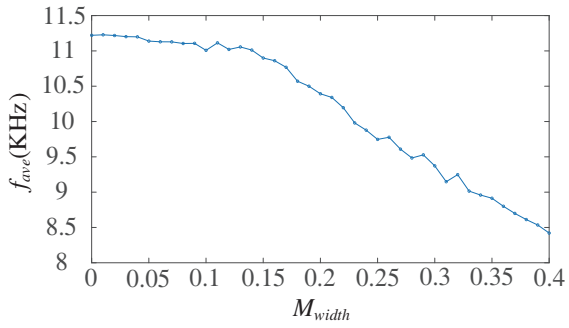

Figure 6. The average switching frequency under different error bands.

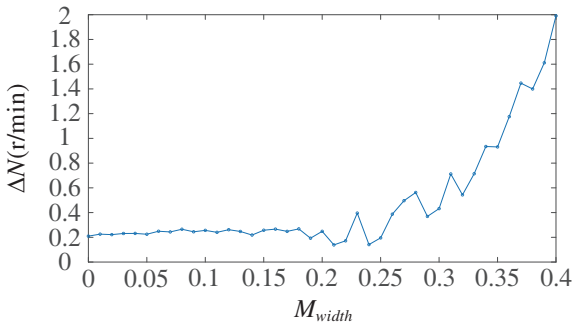

Figure 7. Average rotational speed error under different error bands.

The simulation results have shown that the average switching frequency of the inverter gradually decreased as the hysteresis loop width expanded, but the magnetic chain pulsation and torque pulsation of the motor were increased. When the ratio of the hysteresis loop width is greater than 0.3 times, the model predicts that the control system is biased too strongly in order to reduce the number of switches, and the voltage vector selected at this time cannot meet the performance requirements, resulting in the motor speed not tracking the reference speed properly and the runaway phenomenon. Therefore, considering the control performance of the motor torque and magnetic chain, the fixed hysteresis loop width should be used to avoid selecting too large a proportional multiple of the hysteresis loop width.

Considering the comprehensive performance of the motor, the proportional multiplier of the hysteresis loop width is 0.14 in this paper.

3.5. Introduction of Hysteresis Loops

Uniform experimental conditions were used above in order to properly design the scale M_{width} of the hysteresis loop width. The actual operating conditions of the motor are complex and variable, and it is difficult to match a single hysteresis loop width ratio M_{width} to the variable operating conditions. The design of M_{width} should therefore take into account the current operating conditions of the motor and be adjusted online to achieve optimal control.

Reducing the switching frequency is mainly aimed at introducing the concept of hysteresis loop in MPC control by selecting an appropriate hysteresis loop bandwidth to constrain the stator magnetic chain amplitude and electromagnetic torque inside the hysteresis loop, keeping the output vector constant when it does not exceed the hysteresis loop bandwidth. When the motor operating state changes, the hysteresis loop bandwidth is dynamically output by the fuzzy control.

Given a reference motor speed of 2000 r/min and a load torque TL of 0.1, 0.2, and 0.3 Nm, respectively, the initial value of the hysteresis loop width M_{width} is set to 0, and the M_{width} is gradually increased by a given step (set to 0.01). As the proportional M_{width} of the hysteresis loop width increases, the switching frequency and current distortion rate THD of the inverter are shown in Fig. 8 to Fig. 10.

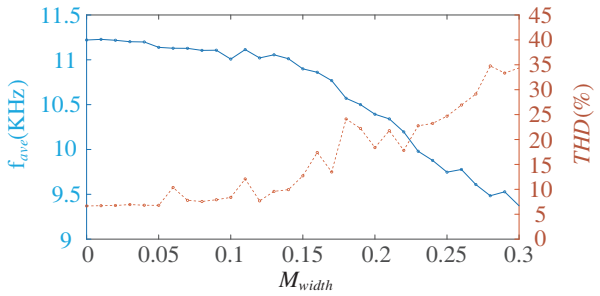

Figure 8. Influence of the hysteresis proportional coefficient M_{width} on the motor performance (TL = 0.1 Nm).

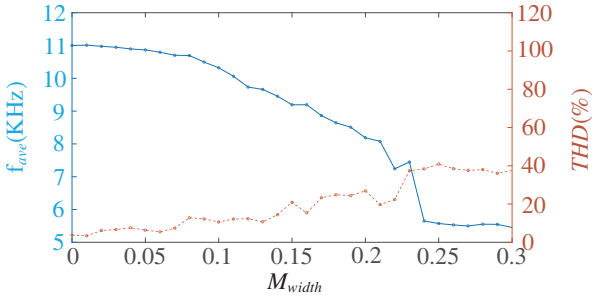

Figure 9. The influence of the hysteresis proportional coefficient M_{width} on the motor performance (TL = 0.2 Nm).

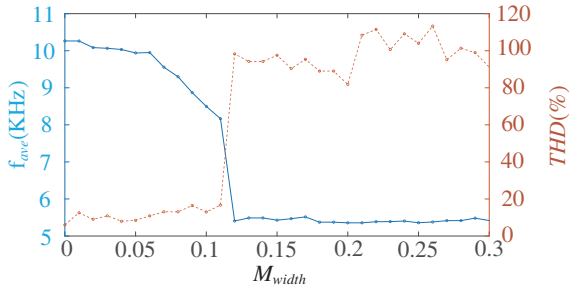

Figure 10. The influence of the hysteresis proportional coefficient M_{width} on the motor performance (TL = 0.3 Nm).

From Fig. 8 to Fig. 10, it can be seen that the combined motor load torque is 0.1, 0.2, and 0.3 Nm, respectively, with the suitable values of [0.08, 0.14] for M_{width}. It can be concluded that the appropriate value of M_{width} is influenced to some extent by the motor torque, which should decrease as the motor torque increases.

Motor torque has a certain influence on the selection of M_{width}. Considering the dynamic response of the motor, attention should be paid to the control of torque and magnetic chain, the width of the hysteresis loop should be reduced to ensure that the system has good dynamic performance. This paper

has introduced a fuzzy algorithm that uses fuzzy control to dynamically output the appropriate M_{width}. The fuzzy controller input variable takes the absolute value of the motor torque $|T_e|$ and speed error Δn.

The absolute motor torque $|T_e|$ domain is [0 Nm, 0.3 Nm], which is divided into four fuzzy subsets, noted as $\{T1, T2, T3, T4\}$, and the affiliation function is shown in Fig. 11.

The speed error Δn has a theoretical domain of [−5 r/min, 5 r/min] and is divided into four fuzzy subsets, noted as $\{N, Z1, Z2, P\}$, with the affiliation function shown in Fig. 12.

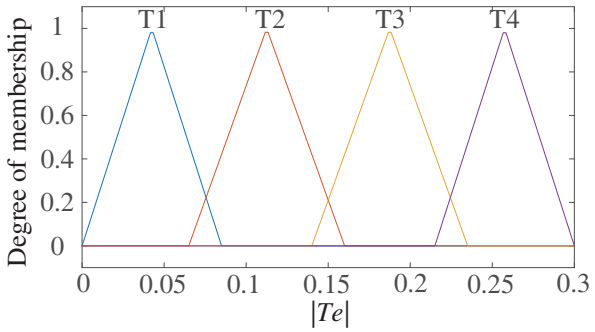

Figure 11. The membership function of the absolute value of the motor torque.

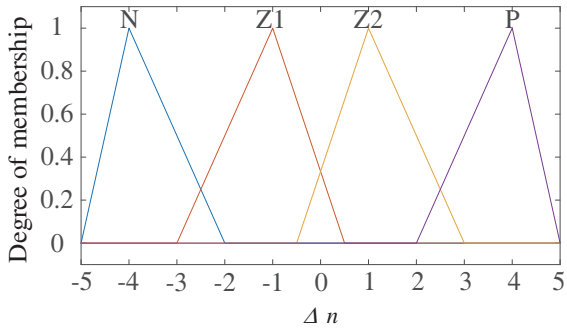

Figure 12. Membership function of speed error.

The multiplicity M_{width} theoretical domain of the hysteresis loop width is [0, 0.14], which is divided into four fuzzy subsets, denoted as {λ1, λ2, λ3, λ4}, and the affiliation function is shown in Fig. 13.

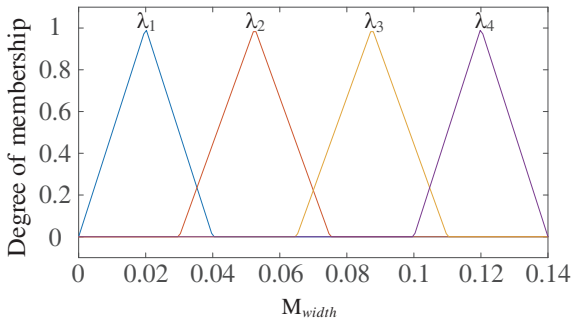

Figure 13. The membership function of the hysteresis width proportional coefficient M_{width}.

From the above it can be obtained that with the increase of motor torque and the absolute value of the motor speed error being too large, the value of M_{width} should be reduced. From the above a fuzzy control table can be obtained, as shown in Table 3. The input-output surface of fuzzy inference is shown in Figure 14. The fuzzy inference input-output surface is shown in Fig. 15.

Table 3. Motor system performance for various hysteresis loop widths.

Δn	$\lvert T_e \rvert$			
	T_1	T_2	T_3	T_4
N	λ_1	λ_1	λ_1	λ_1
Z_1	λ_4	λ_3	λ_2	λ_1
Z_2	λ_4	λ_3	λ_2	λ_1
P	λ_1	λ_1	λ_1	λ_1

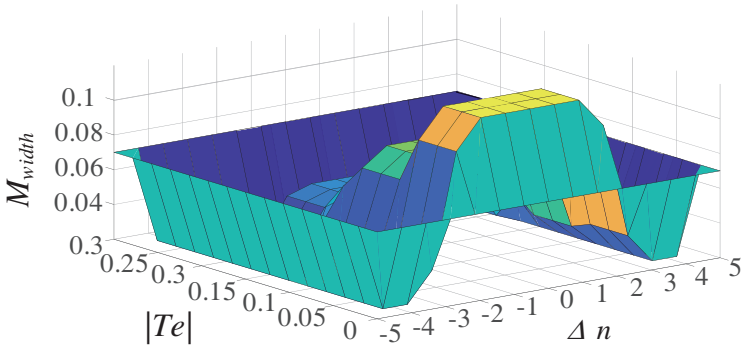

Figure 14. Delayed fuzzy inference input-output surface.

4. EXPERIMENTAL ANALYSIS

In this paper, the proposed improved torque prediction control algorithm is experimentally validated using the RT-LAB experimental platform in Fig. 16. The DSP controller model is TMS320F2812, and the system, inverter, and other parts of the PMSM are built using RT-LAB (op5600).

The PMSM model predicted torque control system used for the experiments remains the same as above, with the PMSM parameters shown in Table 4. The experimental conditions were set as follows: the total duration is 0.5 s. The motor is started from standstill, and the initial speed is given as 100 r/min, with a 0.1 s step to 1000 r/min and a 0.3 s step to 2000 r/min. The initial value of load is 0 Nm, 0.2 s step to 0.1 Nm and 0.3 s step to 0.2 Nm. Three control schemes, namely improved MPTC control with fixed hysteresis width, improved MPTC control with fuzzy variable hysteresis width, and improved MPTC control with fuzzy variable hysteresis width, are used for comparison experiments, and the motor speed, torque, and A-phase current waveforms are shown in Figure 17 to Figure 28, respectively.

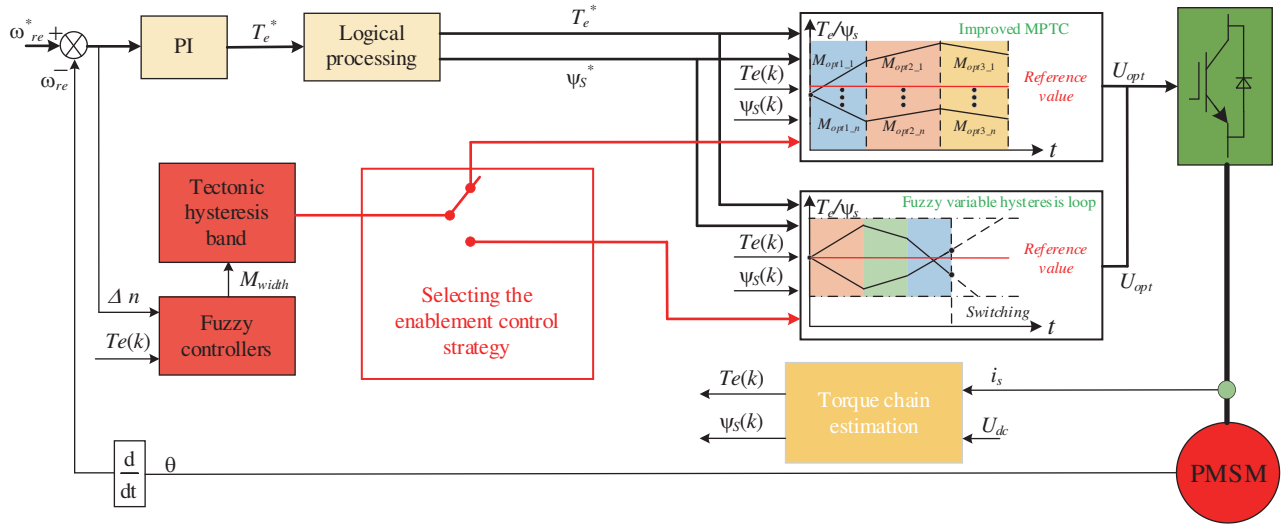

Figure 15. Block diagram of a modified model for predicting torque structure with fuzzy variable hysteresis loop width.

From Table 5 and Fig. 17 to Fig. 19, it can be seen that the speed error of the improved MPTC control strategy is the smallest. Compared with the conventional improved MPTC control strategy, the improved MPTC control strategy with fixed hysteresis loop width and that with fuzzy variable hysteresis loop width increase the speed error to 0.01 r/min and 0.73 r/min, respectively. And the speed

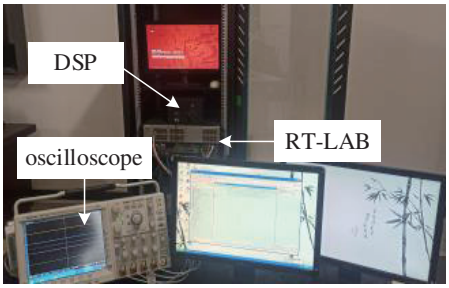

Figure 16. RT-LAB experiment platformer.

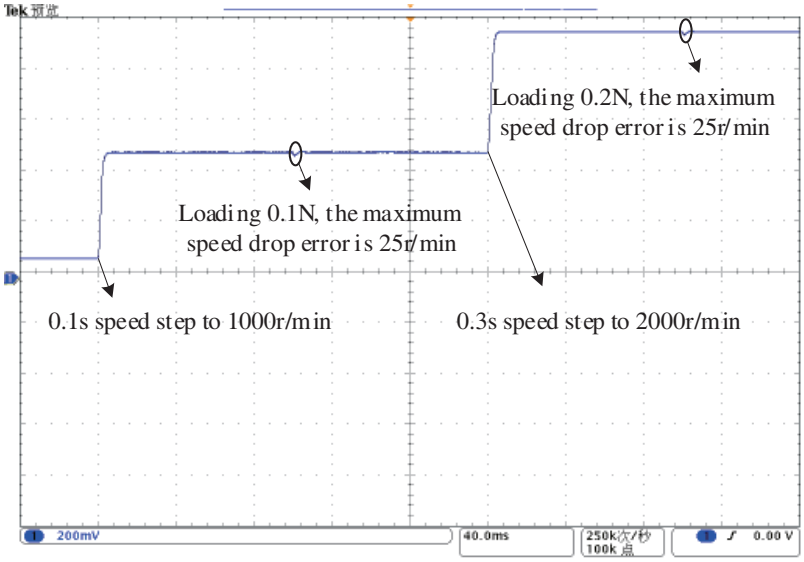

Figure 17. Speed under improved MPTC control.

Table 4. Motor system performance for various hysteresis loop widths.

Parameter	Value	Symbol
Rated power	200 W	P
Permanent magnet flux	0.0105 Wb	Ψ_f
Stator inductance	0.9 mH	L_s
Stator resistance	0.33 Ω	R_s
Rated torque	0.637 Nm	T_N
Rated speed	3000 r/min	N
Inertia	0.0096 Kg·m^2	J
Number of pole pairs	4	P_n

of the fixed hysteresis loop width improved MPTC control strategy has a short runaway phenomenon when stepping up to 2000 r/min.

From Table 5 and Fig. 20 to Fig. 22, it can be seen that the improved MPTC control strategy has the smallest root mean square of motor torque pulsation, and the fixed hysteresis loop width improved MPTC and fuzzy variable hysteresis loop width improved MPTC control strategies have increased

compared to the improved MPTC control strategy, with the root mean square of motor torque pulsation increasing by 0.02 Nm and 0.04 Nm, respectively.

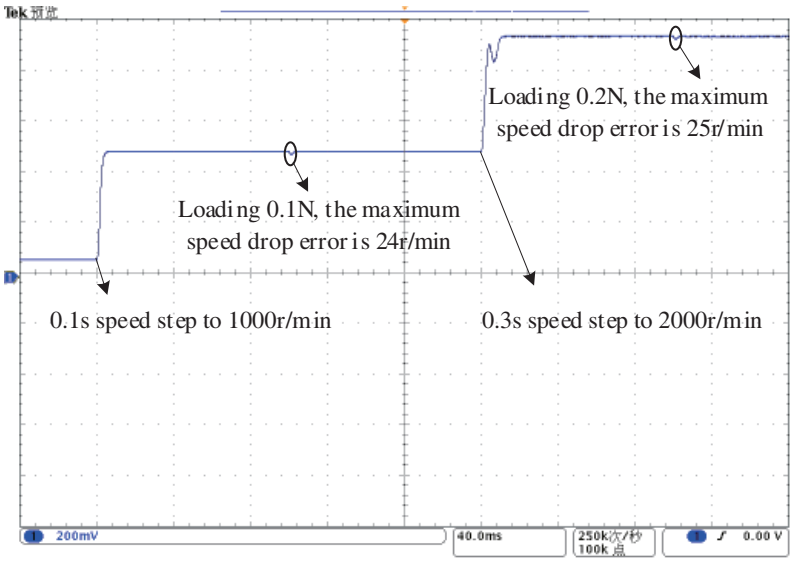

Figure 18. Speed under improved MPTC control with fixed hysteresis width.

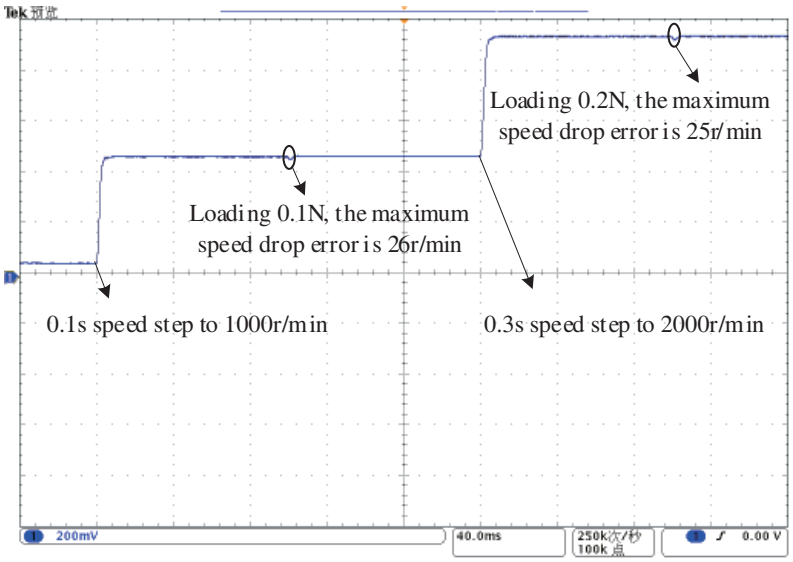

Figure 19. Speed under improved MPTC control with fuzzyvariable hysteresis loop width.

Table 5. Motor system performance under different control strategies.

Control strategies	T_{e_RMSE} (Nm)	ΔN (r/min)	f_{ave} (kHz)
Improved MPTC	0.04	0.13	10.667
Fixed hysteresis loop modified MPTC	0.06	0.14	9.458
Fuzzy variable hysteresis loop improved MPTC	0.08	0.92	8.824

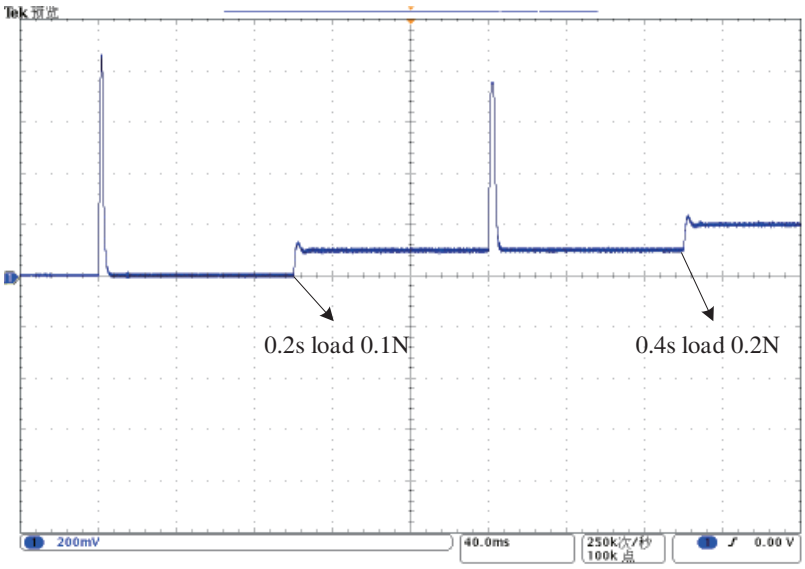

Figure 20. Speed under improved MPTC control with fuzzy variable hysteresis loop width.

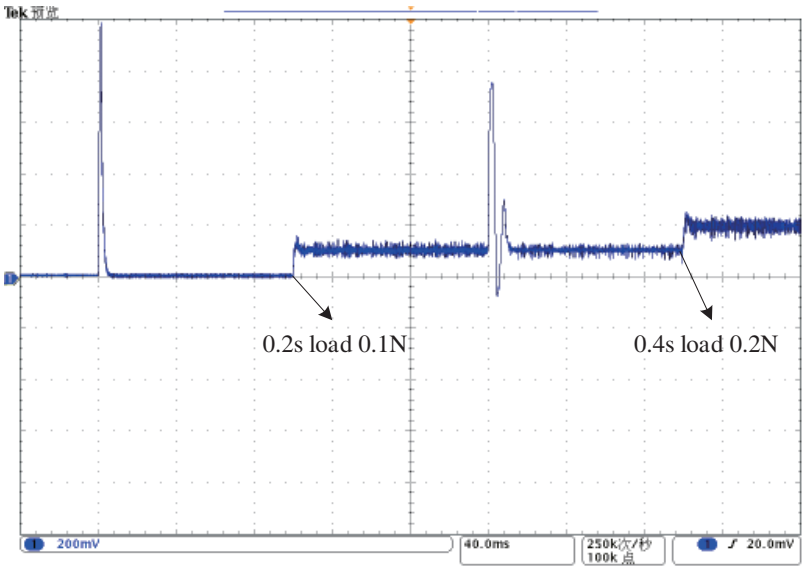

Figure 21. Torque under improved MPTC control with fixed hysteresis width.

Table 6. Steady-state current ripple.

Control strategies	Average switching FREQUENCY (KHZ)	THD (%)	Overall performance Indicators
Improved MPTC	10.666	4.425	11108.5
Fixed hysteresis loop modified MPTC	9.457	29.61	12418
Fuzzy variable hysteresis loop improved MPTC	8.824	12.165	10040.5

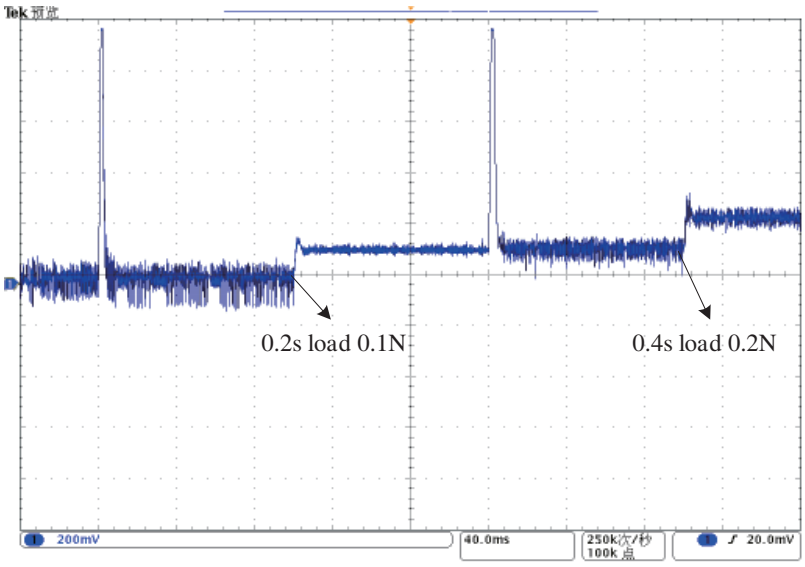

Figure 22. Torque under improved MPTC control with fuzzy variable and fixed hysteresis width.

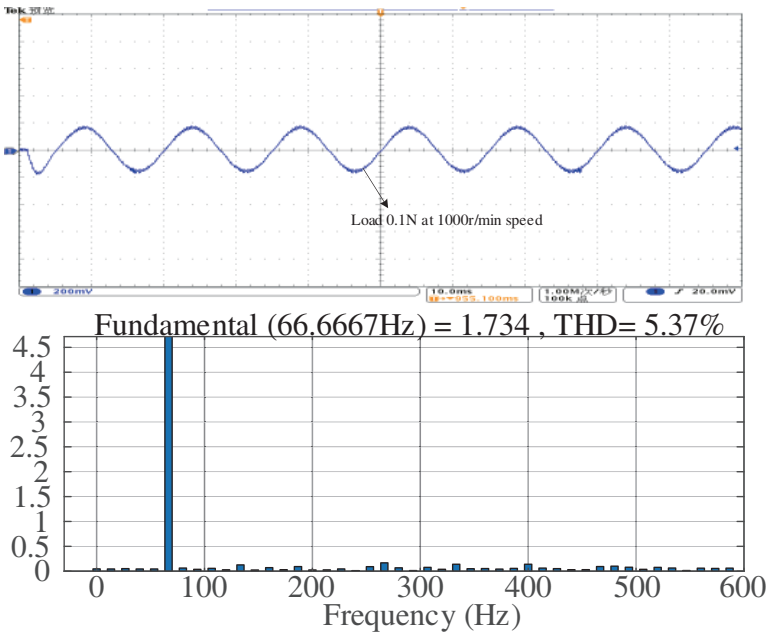

Figure 23. A-phase current and its FFT analysis when loading 0.1 N under the improved MPTC control.

As can be seen from Figures 23 to 28, the stator current distortion rate and inverter switching frequency are two important indicators that need to be balanced, and reducing the current distortion rate and reducing the inverter switching frequency are conflicting indicators.

In order to compare the steady-state performance of the motor when different control strategies are in action, the evaluation index is defined in terms of the order of magnitude difference between the stator current THD and the average switching frequency. The evaluation criterion designed in this paper is the proportion of switching frequency and current distortion 1 : 1 (both are considered equally important), and its purpose is to compare the steady-state performance of the motor when different

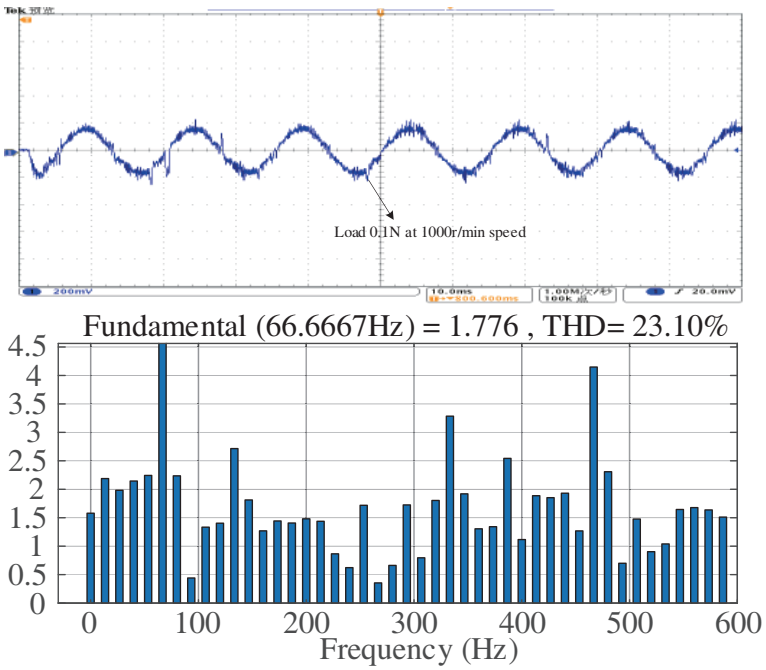

Figure 24. Analysis of A-phase current and FFT at 0.1 N loading under fixed hysteresis loop width improved MPTC control.

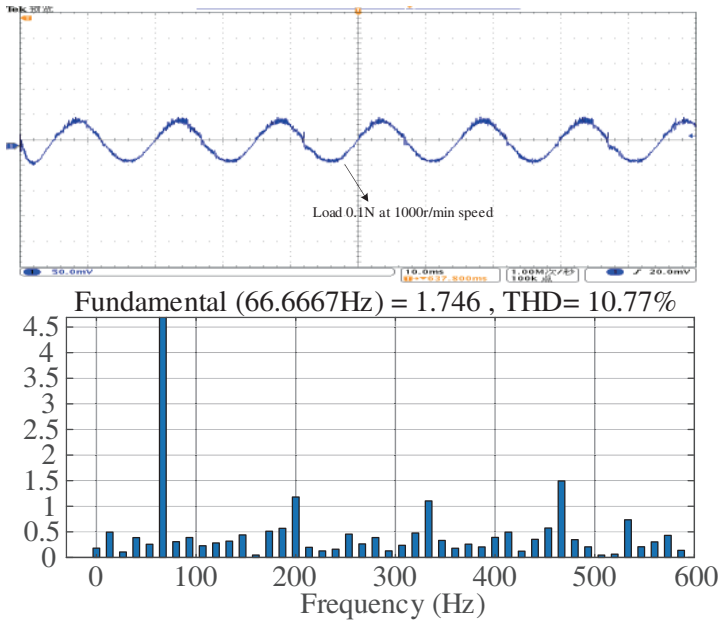

Figure 25. Fuzzy variable fixed hysteresis loop width improved MPTC control with A-phase current at 0.1 N loading and FFT analysis.

control strategies are in action, and when different evaluation indexes are selected, although the data obtained from the calculation will change, the trend of change reflected by them is unchanged [23].

$$S = f_{sw} + 10000 \cdot THD \tag{15}$$

Based on the comprehensive performance index designed in Equation (14), the lower the value of S is, the better the steady-state characteristics of this control strategy are. In Table 6, the current

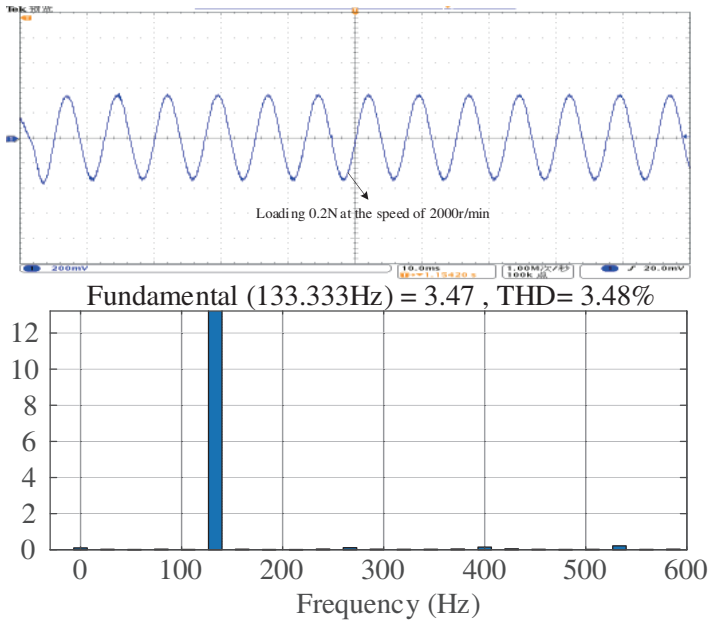

Figure 26. A phase current and its FFT analysis under the loading of 0.2 N under the improved MPTC control.

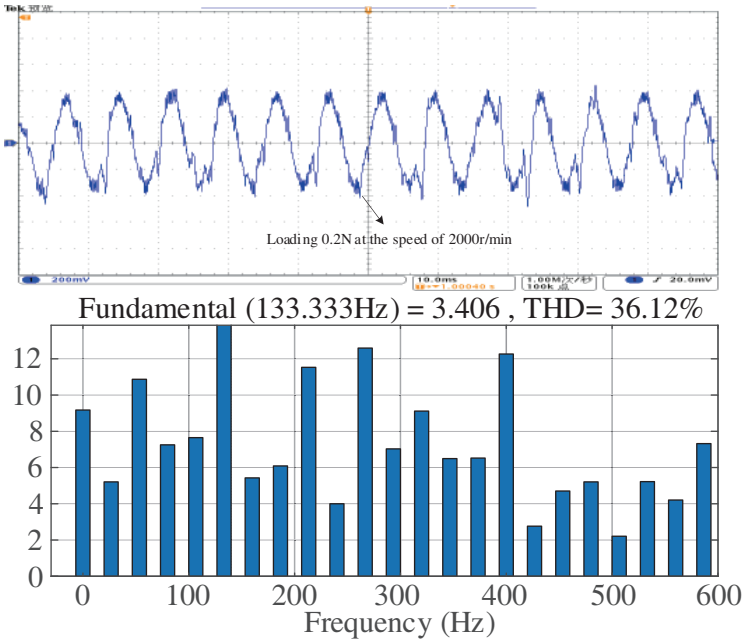

Figure 27. A-phase current and its FFT analysis when 0.2 N is loaded under the improved MPTC control with fixed hysteresis width.

harmonic THD is the average value of current harmonics at loaded 0.1 N and at loaded 0.2 N using different control strategies. The control strategy with fuzzy variable hysteresis loop width has a better effect on the reduction of the switching frequency than the THD. Therefore, the introduction of a fuzzy variable hysteresis loop MPTC control strategy can attenuate the contradiction between the stator current distortion rate and the inverter switching frequency, which is a feature not available in conventional MPTC control strategies.

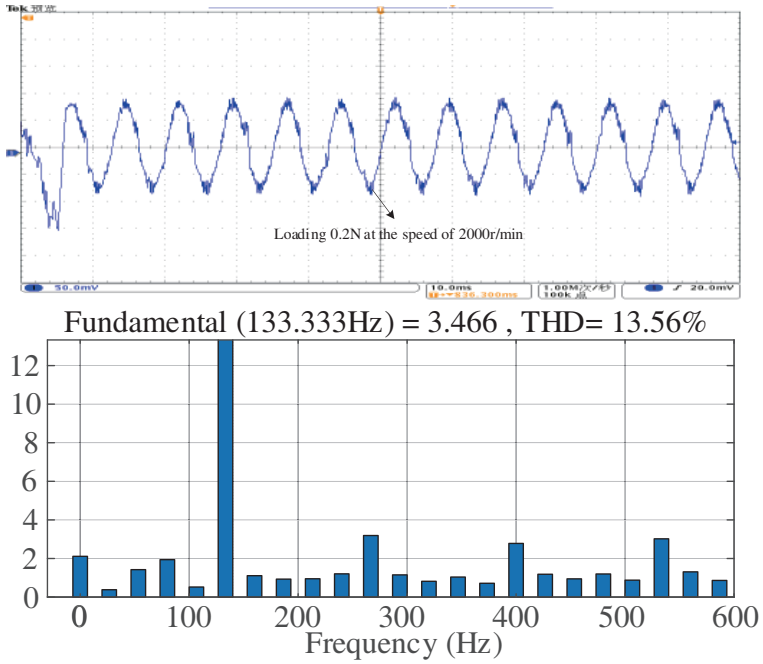

Figure 28. A-phase current and its FFT analysis under 0.2 N loading under the improved MPTC control with fuzzy variable and fixed hysteresis width.

5. CONCLUSION

This paper is aimed at a three-vector predictive control strategy for permanent magnet synchronous motors. The effect of voltage vector combination on the system performance is investigated, and a fuzzy variable hysteresis loop width control strategy is introduced to the improved MPTC algorithm to make the best overall performance under the condition of reducing the switching frequency. The following conclusions are drawn from the experimental results:

1) The combination of the three voltage vectors is selected by an off-line optimized switching table according to the torque control requirements, eliminating the need to calculate the first voltage vector action time and then the other two vector action times, reducing the calculation burden on the system.

2) The concept of direct torque control is introduced on the basis of a modified MPTC control strategy to reduce the average switching frequency. However, in complex operating conditions, the fixed hysteresis loop width cannot be satisfied with a current THD as close to sinusoidal as possible at low switching frequency conditions. The use of a fuzzy variable hysteresis loop width allows the dynamic hysteresis loop width coefficient M_{width} to be output by the fuzzy controller according to the operating state of the motor, reducing the average switching frequency of the inverter on the basis of an improved MPTC control strategy with a fixed hysteresis loop width and at the same time reducing the THD of the current to achieve the best overall performance.

ACKNOWLEDGMENT

This work was supported by the National Natural Science Foundation of China under Grant Number 51907061, Educational Commission of Hunan Province of China under Grant Number 21B0552.

REFERENCES

1. Tong, W., S. Dai, S. Wu, and R. Tang, "Performance comparison between an amorphous metal PMSM and a silicon steel PMSM," *IEEE Transactions on Magnetics*, Vol. 55, No. 6, 1–5, June 2019, Art No. 8102705, doi: 10.1109/TMAG.2019.2900531.
2. Sun, X., Z. Shi, G. Lei, Y. Guo, and J. Zhu, "Analysis and design optimization of a permanent magnet synchronous motor for a campus patrol electric vehicle," *IEEE Transactions on Vehicular Technology*, Vol. 68, No. 11, 10535–10544, Nov. 2019, doi: 10.1109/TVT.2019.2939794.
3. Siami, I. M., D. A. Khaburi, A. Abbaszadeh, and J. Rodríguez, "Robustness improvement of predictive current control using prediction error correction for permanent-magnet synchronous machines," *IEEE Transactions on Industrial Electronics*, Vol. 63, No. 6, 3458–3466, June 2016, doi: 10.1109/TIE.2016.2521734.
4. Zhao, G., J. Feng, and Q. Sun, "The research of optimized torque control algorithm for PMSM based on grey prediction model," *2009 Sixth International Conference on Fuzzy Systems and Knowledge Discovery*, 335–340, 2009, doi: 10.1109/FSKD.2009.588.
5. Chen, W. and D. Sun, "A simplified robust model predictive flux control of open-winding PMSM based on ESO," *2019 22nd International Conference on Electrical Machines and Systems (ICEMS)*, 1–6, 2019, doi: 10.1109/ICEMS.2019.8921676.
6. Zhang, X., K. Yan, and M. Cheng, "Two-stage series model predictive torque control for PMSM drives," *IEEE Transactions on Power Electronics*, Vol. 36, No. 11, 12910–12918, Nov. 2021, doi: 10.1109/TPEL.2021.3075711.
7. Ji, J., R. Xue, W. Zhao, T. Tao, and L. Huang, "Simplified three-vector-based model predictive thrust force control with cascaded optimization process for a double-side linear vernier permanent magnet motor," *IEEE Transactions on Power Electronics*, Vol. 35, No. 10, 10681–10689, Oct. 2020, doi: 10.1109/TPEL.2020.2976901.
8. Sun, X., et al., "MPTC for PMSMs of EVs With multi-motor driven system considering optimal energy allocation," *IEEE Transactions on Magnetics*, Vol. 55, No. 7, 1–6, July 2019, Art No. 8104306, doi: 10.1109/TMAG.2019.2904289.
9. Chen, L., H. Xu, X. Sun, and Y. Cai, "Three-vector-based model predictive torque control for a permanent magnet synchronous motor of EVs," *IEEE Transactions on Transportation Electrification*, Vol. 7, No. 3, 1454–1465, Sept. 2021, doi: 10.1109/TTE.2021.3053256.
10. Luo, Y. and C. Liu, "A flux constrained predictive control for a six-phase PMSM motor with lower complexity," *IEEE Transactions on Industrial Electronics*, Vol. 66, No. 7, 5081–5093, 2019.
11. Huang, W., W. Hua, F. Yin, et al., "Model predictive thrust force control of a linear fluxswitching permanent magnet machine with voltage vectors selection and synthesis," *IEEE Transactions on Industrial Electronics*, Vol. 66, No. 6, 4956–4967, 2019.
12. Lim, C. S., E. Levi, M. Jones, N. Abdul Rahim, and W. P. Hew, "Experimental evaluation of model predictive current control of a five-phase induction motor using all switching states," *2012 15th International Power Electronics and Motion Control Conference (EPE/PEMC)*, LS1c.4-1-LS1c.4-7, 2012, doi: 10.1109/EPEPEMC.2012.6397394.
13. Zhang, Y., B. Xia, and H. Yang, "Performance evaluation of an improved model predictive control with field oriented control as a benchmark," *IET Electric Power Applications*, Vol. 11, No. 5, 677–687, 2017.
14. Ang, Y. L., X. C. Wang, W. Xie, et al., "Deadbeat modelpredictive torque control with discrete space-vector modulation for PMSM drives," *IEEE Transactions on Industrial Electronics*, Vol. 64, No. 5, 3537–3547, 2017.
15. Nasr, A., C. Gu, G. Buticchi, S. Bozhko, and C. Gerada, "A low-complexity modulated model predictive torque and flux control strategy for PMSM drives without weighting factor," *IEEE Journal of Emerging and Selected Topics in Power Electronics*, doi: 10.1109/JESTPE.2022.3152652.
16. Guo, T., Z. Wang, H. Zhang, X. Jiang, and L. Tian, "Cascaded predictive speed control optimization method based on fuzzy controller," *2021 IEEE International Conference on Predictive Control of Electrical Drives and Power Electronics (PRECEDE)*, 328–335, 2021, doi:

10.1109/PRECEDE51386.2021.9680980.

17. Xiang, C., X. Zhang, Z. Li, L. Zhang, and S. Cheng, "Model predict torque control of induction motor based on the DTC switching table," *2020 15th IEEE Conference on Industrial Electronics and Applications (ICIEA)*, 1348–1352, 2020, doi: 10.1109/ICIEA48937.2020.9248310.
18. Hou, L., J. Ma, and W. Wang, "Sliding mode predictive current control of permanent magnet synchronous motor with cascaded variable rate sliding mode speed controller," *IEEE Access*, Vol. 10, 33992–34002, 2022, doi: 10.1109/ACCESS.2022.3161629.
19. Dan, H., P. Zeng, W. Xiong, M. Wen, M. Su, and M. Rivera, "Model predictive control-based direct torque control for matrix converter-fed induction motor with reduced torque ripple," *CES Transactions on Electrical Machines and Systems*, Vol. 5, No. 2, 90–99, June 2021, doi: 10.30941/CESTEMS.2021.00012.
20. Geyer, T., *Model Predictive Control of High Power Converters and Industrial Drives*, John Wiley & Sons, Inc., Chichester, 2016
21. Kim, H., J. Han, Y. Lee, J. Song, and K. Lee, "Torque predictive control of permanent-magnet synchronous motor using duty ratio prediction," *2013 IEEE International Symposium on Industrial Electronics*, 1–5, 2013, doi: 10.1109/ISIE.2013.6563664.
22. Dragičvić, T. and M. Novak, "Weighting factor design in model predictive control of power electronic converters: An artificial neural network approach," *IEEE Transactions on Industrial Electronics*, Vol. 66, No. 11, 8870–8880, Nov. 2019, doi: 10.1109/TIE.2018.2875660.